NUMERICAL PREDICTION OF SHOCK-STANDOFF DISTANCE OF HYPERSONIC WEDGE FLOW AT INCIDENCE

Wilson F. N. Santos

wilson@lcp.inpe.br

Combustion and Propulsion Laboratory

National Institute for Space Research

Cachoeira Paulista, SP, 12630-000, BRAZIL

Abstract. *The aim of the work reported here is to describe the computational investigation of a rarefied hypersonic flow past truncated wedges at incidence. Positive angle-of-attack effect on the shock-wave structure has been investigated by employing the Direct Simulation Monte Carlo (DSMC) method. A method that has become the main technique for studying complex multidimensional rarefied flows, and that properly accounts for the non-equilibrium aspects of the flows. The results presented highlight the sensitivity of the shock-wave standoff distance and shock-wave thickness to changes on the angle of attack as well as on the frontal-face thickness of the leading edges. The analysis showed that positive angle of attack causes the expected asymmetry on the shock-wave patterns as the stagnation point moves from the symmetry axis to the windward side of the leading edges.*

Keywords: Hypersonic flow, Rarefied flow, DSMC, shock standoff, Angle-of-attack.

1. INTRODUCTION

Hypersonic waveriders are advanced hypersonic lifting bodies which generate high values of aerodynamic lift-to-drag ratio at high Mach numbers. Waverider configurations, introduced by Nonweiler (1959), are derived from a known analytical flowfield, such as flow over a two-dimensional wedge or flow around a slender cone. These configurations are designed analytically with infinitely sharp leading edges for shock wave attachment. Because the shock wave is attached to the leading edge of the vehicle, the upper and lower surfaces of the vehicle can be designed separately. Furthermore, the shock wave acts as a barrier in order to prevent spillage of higher-pressure airflow from the lower side of the vehicle to the upper side, resulting in a high-pressure differential and enhanced lift.

Usually, it is extremely difficult to construct a perfectly sharp leading edge. Any manufacturing error results in a significant deviation from the design contour. Moreover, sharp edges are difficult to maintain because they are easily damaged. Additionally, because heat transfer increases inversely with the leading edge radius, high heating is associated with sharp edges. Therefore, for practical hypersonic configurations, leading edges should be blunt for heat transfer, manufacturing and handling concerns. Because blunt leading edge promotes shock wave standoff, practical leading edges will have shock detachment, making leading edge blunting a major concern in the design and prediction of flowfields over hypersonic configurations.

The flowfield properties upstream of the leading edge of a body are affected by molecules reflected from the edge region. The degree of the effect is in part conditioned by the edge geometry. In this context, Santos (2002 and 2005) investigated the effect of the flat-face thickness of truncated wedges on the flowfield structure and on the aerodynamic surface quantities. The thickness effect was examined for a range of Knudsen number, based on the thickness of the flat face, covering from the transitional flow regime to the free molecular flow one. The emphasis of the works was to provide a critical analysis on maximum allowable geometric bluntness, dictated by either handling or manufacturing requirements, resulting on reduced departures from ideal aerodynamic performance of the vehicle. Thus, allowing the blunted leading edge to more closely represents the original sharp leading edge flowfield. Such analysis is also important when a comparison is to be made between experimental results in the immediate vicinity of the leading edge and the theoretical results, which generally assume a zero-thickness leading edge.

Santos (2003) extended further the analysis presented by Santos (2002) on truncated wedges by performing a parametric study on these shapes with emphasis placed on the compressibility effects. The primary goal of the work was to assess the sensitivity of the stagnation point heating, total drag and shock wave standoff distance to changes on the freestream Mach number.

These works (Santos, 2002, 2003 and 2005) on hypersonic flow past truncated wedges have been concentrated primarily on the analysis of the aerothermodynamic surface quantities by considering the diffuse reflection model as being the gas-surface interaction. The diffuse model assumes that the molecules are reflected equally in all directions, quite independently of their incident speed and direction. However, as a space flight vehicle is exposed to a rarefied environment over a considerable time, a departure from the fully diffuse model is observed, resulting from the colliding molecules that clean the surface of the vehicle, which becomes gradually decontaminated. In this connection, Santos (2004) performed a parametric study on truncated wedges with emphasis placed on the gas-surface interaction effects. In this scenario, the primary interest was to assess the sensitivity of the heat transfer and total drag coefficients to variations on the surface accommodation coefficients experienced by the leading edges.

The current proposed paper extends further the previous analysis on truncated wedges by investigating the impact of the angle of attack on the shock-wave structure. For positive angle of attack, important changes occur in the flowfield structure and in the aerodynamic surface quantities on blunt leading edges. This involves the modification of the flowfield properties and shock strength and, consequently, some effects on aerodynamic forces acting on, and on heat transfer to the body surface. Moreover, the knowledge of these properties at zero angle of attack is not sufficient to predict with certainty the flow characteristics over these shapes with incidence. The incidence increase causes an asymmetry in the flow patterns as the stagnation point moves from the symmetry axis to the windward side for positive angle of attack.

In an effort to obtain further insight into the nature of the flowfield structure of truncated wedges under hypersonic transitional flow conditions, the essential characteristics of the angle-of-attack effect on the shock wave will be examined for positive angle of attack with 5, 10, 15 and 20 degrees of incidence.

Under hypersonic transitional flow conditions, at very high speeds and high altitudes, the flow over a given aerodynamic configuration may be sufficiently rarefied that the appropriate molecular mean free path becomes too large, compared to a characteristic length of the vehicle for the use of continuum assumptions but not large enough for the use of the free molecular theory. In such an intermediate or transition rarefied gas regime, where a significant degree of non-equilibrium is observed in the flows, the Direct Simulation Monte Carlo (DSMC) method (Bird, 1994) has been employed in order to solve the problems involving flows of rarefied hypersonic aerothermodynamics.

2. LEADING-EDGE GEOMETRY

The geometry of the leading edges in this work is the same as that presented in previous work (Santos 2005). The truncated wedges are modeled by assuming a sharp leading edge of half angle θ with a circular cylinder of radius R inscribed tangent to this sharp leading edge. The truncated wedges are also tangent to the sharp leading edge and the cylinder at the same common point. It was assumed a leading edge half angle of 10 degrees, a circular cylinder diameter of 10^{-2}m and frontal-face thickness t/λ_∞ of 0.01, 0.1 and 1, where λ_∞ is the freestream mean free path. Figure 1(a) illustrates schematically this construction.

It was assumed that the truncated wedges are infinitely long but only the length L is considered, since the wake region behind the truncated wedges is not of interest in this investigation.
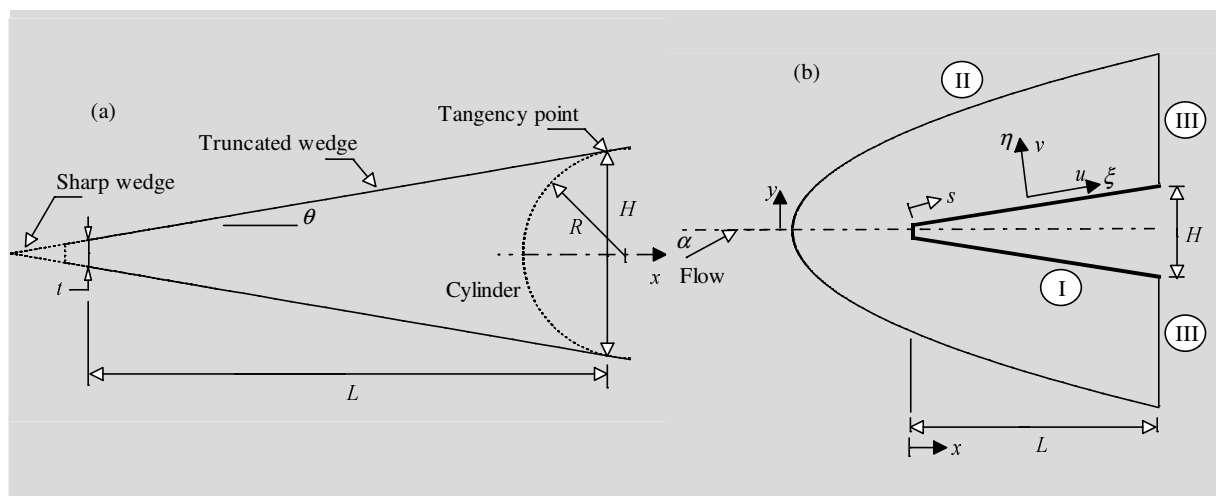

Figure 1: Drawing illustrating (a) the leading edge shapes and (b) the computational domain.

3. COMPUTATIONAL TOOL

The option of the numerical approach in order to model rarefied non-equilibrium flows relies on the extent of flow rarefaction. For near-continuum flows, the boundary conditions of slip velocity and temperature jump are enough to take into account for the rarefaction effects. These boundary conditions are commonly employed in the Navier-Stokes equations or in the viscous shock layer equations. The Navier-Stokes equations can be derived from the Boltzmann equation (Cercignani, 1988) under the assumption of small deviation of the distribution function from equilibrium. Nevertheless, the Navier-Stokes equations become unsuitable for studying rarefied flows where the distribution function becomes considerable non-equilibrium.

In order to study flows with a significant degree of non-equilibrium, the Direct Simulation Monte Carlo (DSMC) method (Bird, 1994), pioneered by Bird in the 60's, has become the standard technique employed.

The DSMC method simulates real gas flows with various physical processes by means of a huge number of modeling particles, each of which is a typical representative of great number of real gas molecules. DSMC models the flow as being a collection of discrete particles, each one with a position, velocity and internal energy. The state of particles is stored and modified with time as the particles move, collide, and undergo boundary interactions in simulated physical space. The simulation is always calculated as unsteady flow. However, a steady flow solution is obtained as the large time state of the simulation. Therefore, the DSMC method is basically an explicit time-marching algorithm.

Collisions in the present DSMC code are modeled by using the variable hard sphere (VHS) molecular model (Bird, 1981) and the no time counter (NTC) collision sampling technique (Bird, 1989). Repartition energy among internal and translational modes is controlled by the Borgnakke-Larsen statistical model (Borgnakke and Larsen, 1975). Simulations are performed using a non-reacting gas model for a constant freestream gas composition consisting of 76.3% of N_2 and 23.7% of O_2. Energy exchanges between the translational and internal modes, rotational and vibrational, are considered. Relaxation collision numbers of 5 and 50 were used for the calculations of rotation and vibration, respectively.

4. COMPUTATIONAL FLOW DOMAIN AND GRID

The computational domain is discretized by using a structured grid. The domain is divided into an arbitrary number of regions, which are subdivided into computational cells. The cells are further subdivided into four subcells, two subcells/cell in each coordinate direction. The linear dimensions of the cells should be small in comparison with the scale length of the macroscopic flow gradients normal to the streamwise directions, which means that the cell dimensions should be of the order of or even smaller than the local mean free path (Alexander et al., 1998 and 2000).

In the current DSMC code, the cell provides a convenient reference for the sampling of the macroscopic gas properties, while the collision partners are selected from the same subcell. As a result, the flow resolution is much higher than the cell resolution. Close to the body surface, cell spacing normal to the body should be also of the order of a third of the local mean free path. If the cell size near the body surface is too large, then energetic molecules at the far edge of the cell are able to transmit momentum and energy to molecules immediately adjacent to the body surface. This leads to overprediction of both the surface heat flux and the aerodynamic forces on the body that would occur in the real gas (Haas and Fallavollita, 1994).

Hence, heat transfer coefficient and pressure coefficient were used as the representative properties for the grid sensitivity study.

Figure 1(b) depicts the physical extent of the computational domain for the present simulations. Based on this figure, side I is defined by the body surface. Diffusion reflection is the condition applied to this side. Side II is the freestream side through which simulated molecules enter and exit. Finally, the flow at the downstream outflow boundary, side III, is predominantly supersonic and vacuum condition is specified (Guo and Liaw, 2001). At this boundary, simulated molecules can only exit.

Numerical accuracy in DSMC method depends on the grid resolution chosen as well as on the number of particles per computational cell. Both effects were investigated to determine the number of cells and the number of particles required to achieve grid independence solutions. The grid generation scheme used in this study follows that procedure presented by Bird (1994). Along the outer boundary (side II) and the body surface (side I) (see Fig. 1(b)), point distributions are generated in such way that the number of points on each side is the same (ξ-direction in Fig. 1(b)). Then, the cell structure is defined by joining the corresponding points on each side by straight lines and then dividing each of these lines into segments which are joined to form the system of quadrilateral cells (η-direction in Fig. 1(b)). The distribution can be controlled by a number of different distribution functions that allow the concentration of points in regions where high flow gradients or small mean free paths are expected.

A grid independence study was made with three different structured meshes in each coordinate direction. The effect of altering the cell size in the ξ-direction was investigated with grids of 50(coarse), 100(standard) and 150(fine) cells, and 60 cells in the η-direction for the bluntest leading edge investigated, $t/\lambda_\infty = 1$ case. In analogous fashion, an examination was made in the η-direction with grids of 30(coarse), 60(standard) and 90(fine) cells, and 100 cells in the ξ-direction for the $t/\lambda_\infty = 1$ case. From the total number of cells in the ξ-direction, 30% are located along the frontal surface and 70% distributed along the afterbody surface. In addition, each grid was made up of non-uniform cell spacing in both directions. The effect (not shown) of changing the cell size in both directions on the heat transfer and pressure coefficients was rather insensitive to the range of cell spacing considered, indicating that the standard grid, 100x60 cells, for the $t/\lambda_\infty = 1$ case, is essentially grid independent. A similar procedure was performed for the other cases investigated.

5. COMPUTATIONAL CONDITIONS

DSMC simulations have been performed for an altitude of 70 km based on the flow conditions given by Santos (2005) and summarized in Table 1, and the gas properties (Bird, 1994) are shown in Table 2. Referring to Tables 1 and 2, T_∞, p_∞, ρ_∞, n_∞, μ_∞, and λ_∞ stand respectively for temperature, pressure, density, number density, viscosity and mean free path, and X, m, d and ω account respectively for mole fraction, molecular mass, molecular diameter and viscosity index.

The freestream velocity V_∞ is assumed to be constant at 3.56 km/s, which correspond to a freestream Mach number M_∞ of 12. The translational and vibrational temperatures in the freestream are in equilibrium at 220 K, and the wedge surface has a constant wall temperature T_w of 880 K for all cases considered. This temperature is chosen to be representative of the surface temperature near the stagnation point and is assumed to be uniform over the bodies.

The overall Knudsen number Kn is defined as the ratio of the molecular mean free path λ in the freestream gas to a characteristic dimension of the flowfield. In the present account, the characteristic dimension was defined as being the thickness t of the frontal face of the leading edges. For the thicknesses investigated, $t/\lambda_\infty = 0.01$, 0.1 and 1, the overall Knudsen numbers

correspond to Kn_t = 100, 10, and 1. Finally, the Reynolds number Re_t covers the range from 0.193 to 19.3, based on conditions in the undisturbed stream with leading edge thickness t as the characteristic length.

Table 1: Freestream Conditions

Altitude (km)	T_∞ (K)	p_∞ (N/m^2)	ρ_∞ x 10^5 (kg/m^3)	n_∞ x 10^{-21} (m^{-3})	μ_∞ x 10^5 (Ns/m^2)	λ_∞ x 10^3 (m)	V_∞ (m/s)
70	220.0	5.582	8.753	1.8209	1.455	0.903	3560

Table 2: Gas Properties

	X	m (kg)	d (m)	ω
O_2	0.237	5.312 x 10^{-26}	4.01 x 10^{-10}	0.77
N_2	0.763	4.65 x 10^{-26}	4.11 x 10^{-10}	0.74

In order to simulate the angle-of-attack effect, the DSMC calculations were performed independently for five distinct numerical values of α, i.e., 0, 5, 10, 15 and 20 degrees. It is important to mention that α equal to 0 represents the case investigated previously (Santos, 2005).

6. COMPUTATIONAL PROCEDURE

The problem of predicting the shape and location of detached shock waves has been stimulated by the necessity for blunt noses and leading edges configurations designed for hypersonic flight in order to cope with the aerodynamic heating. In addition, the ability to predict the shape and location of shock waves is of primary importance in analysis of aerodynamic interference. Furthermore, the knowledge of the shock wave displacement is especially important in waveriders (Nonweiler, 1959), since these hypersonic configurations usually rely on shock wave attachment at the leading edges to achieve their high lift-to-drag ratio at high-lift coefficient.

In this present account, the shock-wave structure, defined by shape, thickness and detachment of the shock wave, is predicted by employing a procedure based on the physics of the particles. In this respect, the flow is assumed to consist of three distinct classes of molecules; class I molecules denote those molecules from freestream that have not been affected by the presence of the leading edge; class II molecules designate those molecules that, at some time in their past history, have struck and been reflected from the body surface; and finally, class III molecules define those molecules that have been indirectly affected by the presence of the body. Figure 2(a) illustrates the definition for the molecular classes.

It is assumed that the class I molecule changes to class III molecule when it collides with class II or class III molecule. Class I or class III molecule is progressively transformed into class II molecule when it interacts with the body surface. Also, a class II molecule remains class II regardless of subsequent collisions and interactions. Hence, the transition from class I molecules to class III molecules may represent the shock wave, and the transition from class III to class II may define the boundary layer.

A typical distribution of class III molecules along the stagnation streamline for blunt leading edges is displayed in Fig. 2(b) along with the definition used to determine the thickness, displacement and shape of the shock wave. In this figure, X is the distance x along the stagnation streamline (see Fig. 1(b)), normalized by the freestream mean free path λ_∞, and

f_{III} is the number of molecules for class III to the total amount of molecules inside each cell.

In a rarefied flow, the shock wave has a finite region that depends on the transport properties of the gas, and it can no longer be considered as a discontinuity obeying the classical Rankine-Hugoniot relations. In this context, the shock standoff distance Δ is defined as being the distance between the shock wave center and the nose of the leading edge along the stagnation streamline. As shown in Fig. 2(b), the center of the shock wave is defined by the station that corresponds to the maximum value for f_{III}. The shock wave thickness δ is defined by the distance between the stations that correspond to the mean value for f_{III}. Finally, the shock wave shape (shock wave "location") is determined by the coordinate points given by the maximum value in the f_{III} distribution along the lines departing from the body surface, i.e., η-direction as shown in Fig. 1(b).
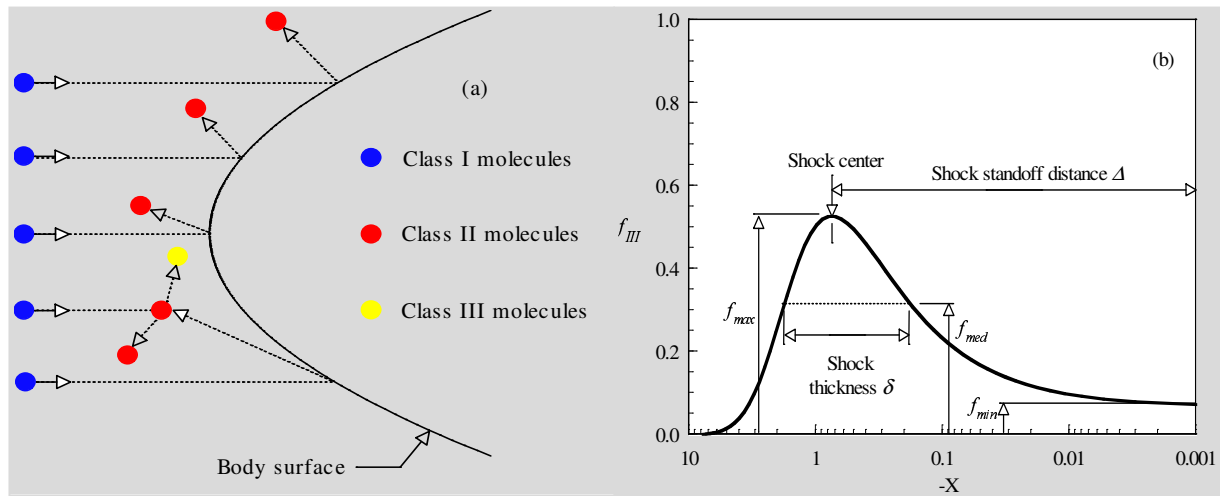

Figure 2: (a) Drawing illustrating the classification of molecules and (b) Schematic of shock wave structure.

7. COMPUTATIONAL RESULTS AND DISCUSSION

The purpose of this section is to discuss and to compare differences in the displacement, thickness and shape of the shock wave due to variations on the angle of attack as well as on the leading edge thickness. Before proceeding with the analysis of the shock-wave structure, it is desirable to highlight the major features of the results related to the molecular class distribution.

7.1 Molecular Class Distribution

The distribution of molecules for classes I, II and III along the symmetry line is illustrated in Figs. 3(a) and 3(b) for thickness Knudsen number Kn_t of 100 and 1 (t/λ_∞ of 0.01 and 1), respectively. These figures display the distribution of molecules for angle of attack of 0 and 20 degrees. Nevertheless, it should be also mentioned that increasing the incidence causes the expected asymmetry in the flow patterns as the stagnation point moves from the symmetry axis to the lower windward side of the leading-edge surface. In this scenario, it proves instructive to illustrate the molecular class distribution along the new stagnation streamline. Therefore, for comparison purpose, the distribution of molecules for classes I, II and III along the stagnation line are displayed in Figs. 4(a) and 4(b) for Kn_t of 100 and 1, respectively. The class distributions for the other cases investigated in this work are intermediate to the cases displayed in this set of figures and, therefore, they will not be shown.

Referring to Figs. 3(a) and 3(b), f_I, f_{II} and f_{III} are the ratio of the number of molecules for class I, II and III, respectively, to the total amount of molecules inside each cell along the symmetry line. Also, the curves with full and empty symbols correspond to angle of attack α of 0 and 20 degrees, respectively.
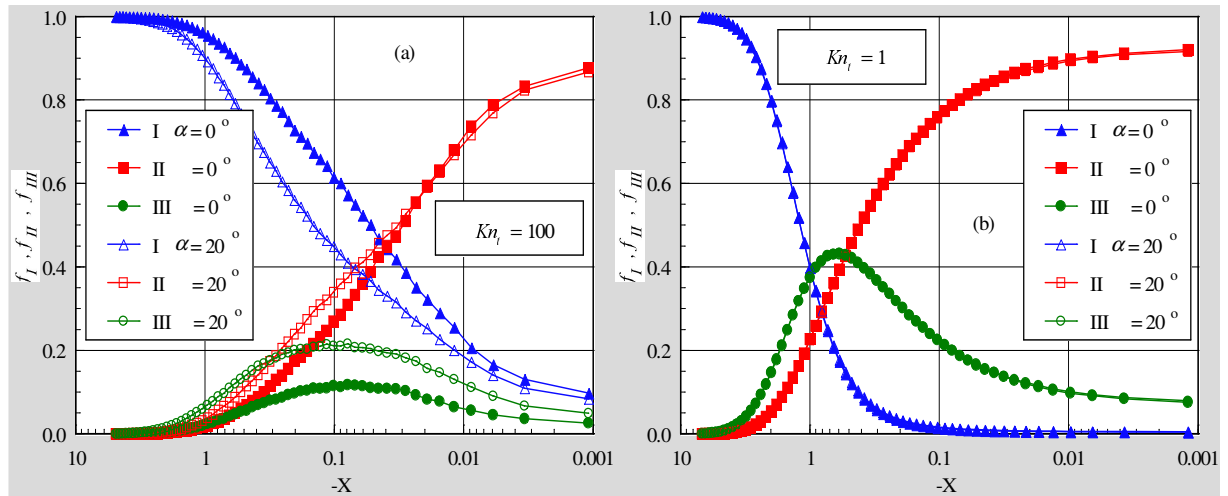

Figure 3: Distributions of molecules for classes I, II and III along the symmetry line parameterized by the angle of attack for thickness Knudsen number Kn_t of (a) 100 and (b) 1.
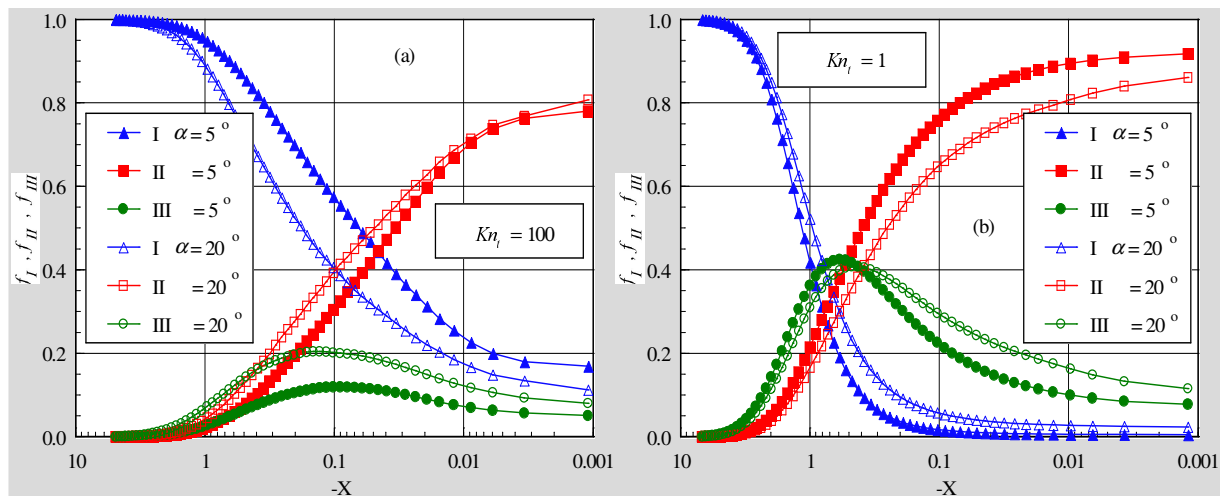

Figure 4: Distributions of molecules for classes I, II and III along the stagnation streamline parameterized by the angle of attack for thickness Knudsen number Kn_t of (a) 100 and (b) 1.

Of great significance in Figs. 3(a) and 3(b) is the behavior of the class I molecules for sharp and blunt leading edges. It should be observed that molecules from freestream, represented by class I molecules, collide with the nose of the leading edges even after the establishment of the steady state. This is shown in Fig. 3(a), which represent the sharp leading edge case. In contrast, molecules from freestream basically do not reach the nose of the leading edge for those cases illustrated in Fig. 3(b), which represent blunt leading edges. This is explained by the fact that density increases much more at the vicinity of the stagnation region for blunt leading edges (Santos, 2006), and reaches its maximum value in the stagnation point for the case of zero degree of incidence. In this connection, the buildup of particle density near the nose of the leading edge acts as a shield for the molecules coming

from the undisturbed stream. It may be recognized from Figs. 3(a) and 3(b) that the angle-of-attack effect on the shock standoff distance and on the shock thickness is more pronounced for the leading edge case defined by Kn_t of 100 than that for Kn_t of 1. Basically no appreciable changes on both properties are observed for Kn_t of 1 along the symmetry line. Nevertheless, appreciable changes on the shock standoff distance and on the shock thickness are observed along the stagnation streamline for the angle-of-attack variation investigated, as illustrated by Figs. 4(a) and 4(b).

7.2 Shock-Wave Standoff Distance

The shock wave standoff distance Δ can be observed in Figs. 3 and 4 for the cases shown. Based on the shock displacement definition presented in Fig. 2(b), the calculated shock wave standoff distance Δ, normalized by the freestream mean free path λ_∞, is tabulated in Table 3 for the cases investigated. As mentioned previously, due to the angle-of-attack effect, the stagnation streamline moves from the symmetry line to a new position in the windward side. In this way, Table 3 tabulates the shock standoff distance along the symmetry line and along the stagnation line. The stagnation-line data are shown inside the parenthesis.

Table 3: Dimensionless shock wave standoff distance Δ/λ_∞ along the symmetry line and stagnation line for truncated wedges at incidence.

α (degree)	$Kn_t = 100$	$Kn_t = 10$	$Kn_t = 1$
0	0.076	0.231	0.603
5	0.081 (0.097)	0.202 (0.192)	0.605 (0.584)
10	0.092 (0.090)	0.227 (0.213)	0.607 (0.503)
15	0.092 (0.110)	0.230 (0.208)	0.606 (0.453)
20	0.098 (0.135)	0.233 (0.243)	0.607 (0.450)

It is apparent from the results on Table 3 that there is a discrete shock standoff distance for the cases shown. As would be expected, the shock standoff distance increases with increasing the leading-edge thickness; since the leading edge becomes blunt with increasing the frontal thickness t. It is also seen that, the shock standoff distance along the symmetry line increased with increasing the angle of attack for thickness Knudsen numbers of 100 and 10. In contrast, no appreciable changes were observed for thickness Knudsen number of 1 at incidence.

It is important to mention that shock standoff distance becomes important in hypersonic vehicles such as waveriders, which depend on leading edge shock attachment to achieve their high lift-to-drag ratio at high lift coefficient. In this connection, leading edge with smaller frontal face seem to be more appropriate, since it presents reduced shock wave detachment distances. Although it has long been known that smaller shock detachment distance is associated with a higher heat load to the nose of the body.

7.3 Shock-Wave Thickness

According to the definition for shock-wave thickness illustrated in Fig. 2(b), the shock wave thickness δ along the stagnation streamline can be calculated from Figs. 3 and 4 for the leading edges cases displayed. As a result of the calculation, Table 4 tabulates the shock-wave thickness δ, normalized by the freestream mean free path λ_∞, for all cases investigated. In a similar way, the values presented are for the shock-wave thickness along the symmetry line and the stagnation line.

It is evident from Table 4 that, in general, the shock-wave thickness follows the same trend presented by the shock-wave standoff distance in that it increases with increasing the angle of attack α for thickness Knudsen numbers of 100 and 10, and stays constant for thickness Knudsen number of 1.

Table 4: Dimensionless shock wave thickness δ/λ_∞ along the symmetry line and stagnation line for truncated wedges at incidence.

α (degree)	$Kn_t = 100$	$Kn_t = 10$	$Kn_t = 1$
0	0.367	0.530	1.349
5	0.382 (0.318)	0.538 (0.460)	1.344 (1.313)
10	0.410 (0.357)	0.566 (0.492)	1.348 (1.238)
15	0.452 (0.412)	0.595 (0.540)	1.351 (1.131)
20	0.519 (0.474)	0.643 (0.594)	1.354 (1.212)

7.4 Shock-Wave Shape

The shock-wave shape, defined by the shock wave center location, is obtained by calculating the position that corresponds to the maximum f for class III molecules in the η-direction along the body surface (see Fig. 2(b)). Comparison of the shock wave shape at incidence and at zero angle of attack is illustrated in Fig. 5(a) for thickness Knudsen number of 1. In an effort to emphasize points of interest, a magnified view of the shock wave shapes at the vicinity of the leading-edge nose is shown in Fig. 5(b). In this set of plots, X and Y are the Cartesian coordinates x and y normalized by λ_∞.
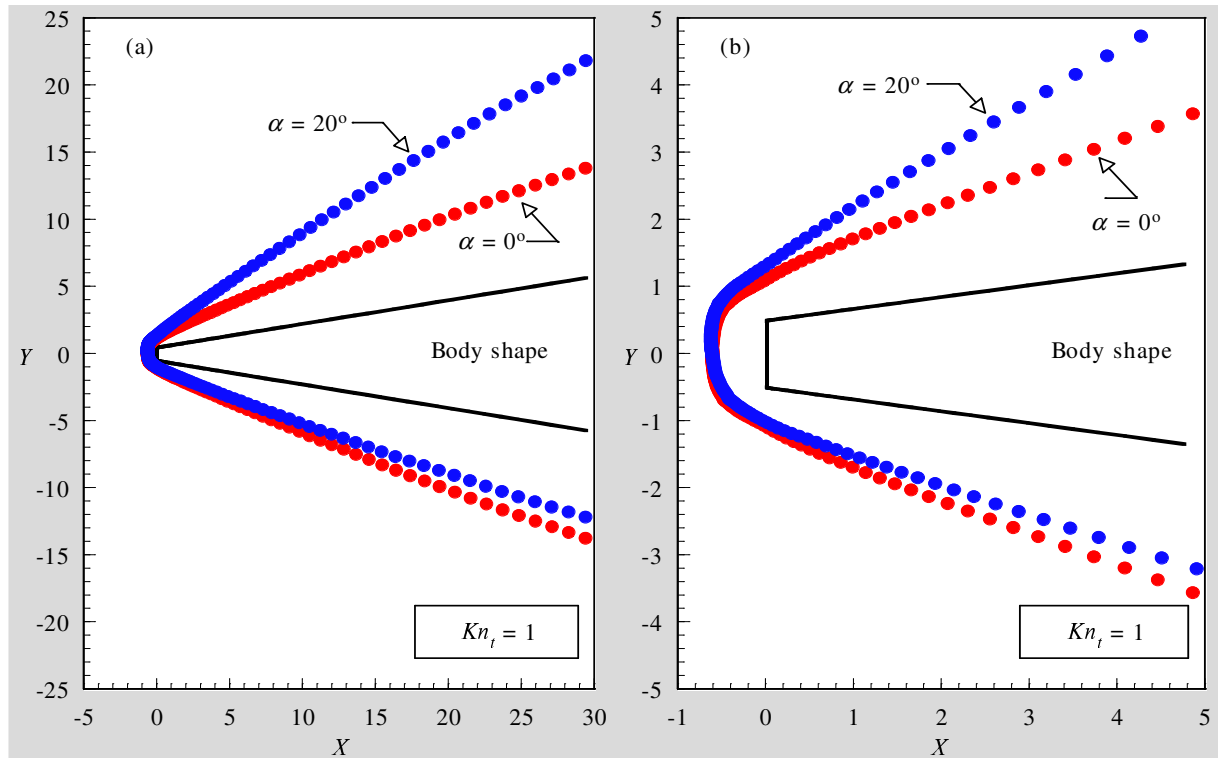

Figure 5: Shock-wave shapes on truncated wedges as a function of the angle of attack for thickness Knudsen number Kn_t of 1: (a) shock-wave on the total leading edge and (b) magnified view at the vicinity of the leading-edge nose.

It is seen from this set of figures that increasing the incidence causes the expected asymmetry in the shock wave patterns as the stagnation point moves from the axis to the lower windward side. As a result, the net buildup of particle density decreases in the leeward side and it increases in the windward side (Santos, 2006) with increasing the incidence. Consequently, the presence of the leading edge, propagated by random motion of the molecules, is communicated to a larger distance away from the body in the leeward side than that in the windward side. Hence, the shock wave center locates more away of the body surface on the leeward side and closer to the body surface on the windward side.

8. CONCLUDING REMARKS

This study applies the Direct Simulation Monte Carlo method to investigate the shock wave structure for a family of truncated wedges. The calculations have provided information concerning the nature of the shock-wave detachment distance, shock-wave thickness and shock-wave shape resulting from variations on the angle of attack and on the thickness of the frontal face for the idealized situation of two-dimensional hypersonic rarefied flow.

The analysis showed that the shock-wave structure was affected by changes on the angle of attack. It was found that the shock-wave standoff and the shock-wave thickness increased with the incidence rise for the sharp leading edge cases investigated. In contrast, no appreciable changes were observed in both properties for the blunt leading edge case. As expected, it was also verified that the shock wave center locates more away of the body surface on the leeward side than that on the windward side.

REFERENCES

Alexander, F. J., Garcia, A. L., & Alder, B. J., 1998, Cell size dependence of transport coefficient in stochastic particle algorithms. *Physics of Fluids*, vol. 10, n. 6, pp. 1540-1542.

Alexander, F. J., Garcia, A. L., & Alder, B. J., 2000, Erratum: Cell size dependence of transport coefficient is stochastic particle algorithms. *Physics of Fluids*, vol. 12, n. 3, pp. 731-731.

Bird, G. A., 1981, Monte Carlo simulation in an engineering context. In Sam S. Fisher, ed., *Progress in Astronautics and Aeronautics: Rarefied gas Dynamics*, vol. 74, part I, pp. 239-255, AIAA, New York.

Bird, G. A., 1989, Perception of numerical method in rarefied gasdynamics. In E. P. Muntz, and D. P. Weaver and D. H. Capbell, eds., *Rarefied gas Dynamics: Theoretical and Computational Techniques*, vol. 118, pp. 374-395, Progress in Astronautics and Aeronautics, AIAA, New York.

Bird, G. A., 1994, *Molecular Gas Dynamics and the Direct Simulation of Gas Flows*. Oxford University Press, Oxford, England, UK.

Borgnakke, C. & Larsen, P. S., 1975, Statistical collision model for Monte Carlo simulation of polyatomic gas mixture. *Journal of computational Physics*, vol. 18, n. 4, pp. 405-420.

Cercignani, C., 1988, *The Boltzmann Equation and Its Applications*, Springer-Verlag, New York, NY.

Garcia, A. L., & Wagner, W., 2000, Time step truncation error in direct simulation Monte Carlo. *Physics of Fluids*, vol. 12, n. 10, pp. 2621-2633.

Guo, K. & Liaw, G.-S., 2001, A review: boundary conditions for the DSMC method. In *Proceedings of the 35th AIAA Thermophysics Conference*, AIAA Paper 2001-2953, Anaheim, CA.

Haas, B, L., & Fallavollita, M. A., 1994, Flow resolution and domain influence in rarefied hypersonic blunt-body flows. *Journal of Thermophysics and Heat Transfer*, vol. 8, n. 4, pp. 751-757.

Hadjiconstantinou, N. G., 2000, Analysis of discretization in the direct simulation Monte Carlo. *Physics of Fluids*, vol. 12, n. 10, pp. 2634-2638.

Nonweiler, T. R. F., 1959, Aerodynamic problems of manned space vehicles. *Journal of the Royal Aeronautical Society*, vol. 63, Sept, pp. 521-528.

Santos, W. F. N., 2002, Truncated leading edge effects on flowfield structure of a wedge in low density hypersonic flight speed. In *9th Brazilian Congress of Thermal Engineering and Sciences, ENCIT 2002*, Caxambu, MG, Brazil.

Santos, W. F. N., 2003, Compressibility effects on flowfield structure of truncated leading edge in low density hypersonic flow. In *17th International Congress of Mechanical Engineering*, *COBEM 2003*, São Paulo, SP, Brazil.

Santos, W. F. N., 2004, The effect of incomplete surface accommodation on heat transfer and drag of truncated wedge in rarefied regime. In *3rd Brazilian Congress of Mechanical Engineering, CONEM 2004*, Belém, PA, Brazil.

Santos, W. F. N., 2005, Flat-faced leading-edge effects in low-density hypersonic wedge flow, *Journal of Spacecraft and Rockets*, vol. 42, n. 1, pp. 22-29.

Santos, W. F. N., 2006, Angle-of-attack effect on rarefied hypersonic wedge flow. In *VII Simposium of Computational Mechanics, SIMMEC 2006*, Araxá, MG, Brazil.